International Journal of
INTELLIGENT SYSTEMS AND APPLICATIONS IN ENGINEERING
ISSN:2147-6799 www.ijisae.org Original Research Paper

Efficient Brain Tumor Identification Based on Optimal Support Scaling Vector Feature Selection (OSSCV) Using Stochastic Spin-Glass Model Classification

J. Veneeswari[1*], S. Sankar Ganesh[2], Lalitha Krishnasamy[3], T. Rengaraj[4], D. Suseela[5], N. Kumaran[6]

Submitted: 03/11/2023 **Revised**: 22/12/2023 **Accepted**: 04/01/2024

Abstract: Brain tumor detection is a developing defect finding task in medical imaging, as premature and early identification is a critical once for recommending early treatment. The tumor are identified by the laboratory through MRI images by finding the tumor regions. The Artificial intelligence play a vital role for finding, analyzing, the image data to attain the target results in medical image using various learning methodologies. Most of the existing system failed to find the find the feature dimension leads poor accuracy for identifying tumor regions due to low precision, recall rate, lower intensity in image coverage region. To resolve this problem, to propose an Optimal Support Scaling Vector Based Feature Selection (OSSCV) brain tumor identification using Stochastic Spin-Glass Model Classification (SSGM). Initially the preprocessing is done by bilateral filter and segmentation is applied by suing Active Region Slice Window Segmentation (ARSWS). To separate the tumor entity feature projection using Histogram color quantization and the features process are carried by Optimal Support Scaling Vector Based Feature Selection (OSSCV). The selected features get trained using Stochastic Spin-Glass Model Classification (SSGM) to find the tumor region. The proposed system outperforms traditional machine learning methods in brain tumor detection. Finally proposed system of Stochastic Spin-Glass Model (SSGM) performance of recall is 95.5%, the performance of F1-score is 96.1% and the performance of the 96.5%. The proposed approach has the potential to assist radiologists in diagnosing brain tumors more accurately and efficiently, leading to improved patient outcomes.

Keywords: *Machine learning, brain tumor, feature selection, classification, neural network, stochastic spin model, MRI image processing*

1. Introduction

Detecting brain tumors is a crucial focus of medical imaging research, as it significantly impacts early diagnosis and treatment planning for patients undergoing brain MRI scans. Magnetic resonance imaging (MRI) serves as a extensively utilized imaging method for diagnosing brain tumors, offering comprehensive anatomical details [1]. Brain tumors, characterized by abnormal cell growth within the brain, can be either benign or malignant, making their early identification essential for successful treatment. Nevertheless, interpreting MRI images to detect brain tumors presents a challenging and time-intensive task for radiologists,often resulting in diagnostic accuracy variability.

This proposed methodology introduces a comprehensive method for identifying brain tumors in magnetic resonance imaging (MRI) scans, incorporating segmentation, histogram assessment, feature selection, and classification methodologies. The proposed approach entails segmenting brain tumor areas, extracting and selecting features based on histograms, and training a classification prototypical to discriminate between tumor and non-tumor regions [2]. The experimental findings showcase the efficacy of this integrated approach in precisely detecting brain tumors in MRI images, underscoring its potential to improve diagnostic precision and treatment planning.

The method proposed employs feature selection and classification to automatically learn and extract distinguishing features from pre-processed MRI images. Our approach's effectiveness is demonstrated through experimental results, indicating its superior performance compared to the previous methods by identifying the brain tumors. Figure 1 illustrates the process of brain tumor feature selection and classification. The feature selection reduces the dimensionality ratio of affected brain tumor

1Assistant Professor, Department of Information Technology, iNurture Education Solutions Private Limited, Vels University, Chennai-600117. Tamil Nadu, India.Email: veneeswari26@gmail.com

2.Associate Professor, Department of Computer Science and Engineering, Kommuri Pratap Reddy Institute of Technology, Medchal, Hyderabad - 501301. Telangana, India. Email: sankar2017vmu@gmail.com

3 Associate Professor Department of CSE, School of Engineering and Technology, Christ (Deemed to be) University, Bengaluru -560074. Email: vrklalitha24@gmail.com

[4]Assistant Professor,Department of Electrical and Electronics Engineering, P. S. R Engineering College, Sevalpatti, Sivakasi-626140, Tamil Nadu, India. Email: rajpriya160619@gmail.com

[5]Assistant Professor,Department of Artificial Intelligence and Machine Learning, Bannari Amman Institute of Technology Sathyamangalam-638401, Tamil Nadu,India. Email: suseelamtech15@gmail.com

[6]Assistant Professor, Department of Mathematics, Veltech Rangarajan Dr.Sagunthala R&D institute of science and technology,Avadi, Chennai – 600062,Tamil Nadu,India.Email : nkumaran@veltech.edu.in

areas more accurately and efficiently, ultimately contributing to enhanced patient outcomes.

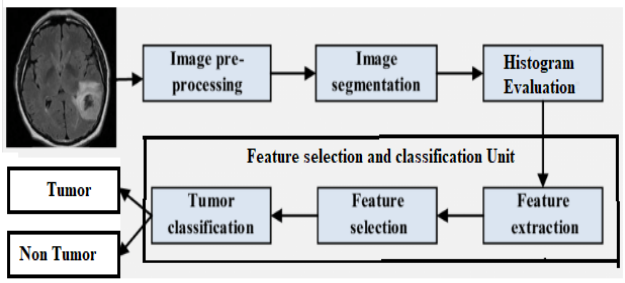

Fig 1: Brain tumor feature selection and classification process.

The feature selection and classification has proven the remarkable success in analyzing medical images, particularly in tumor detection [3]. DL techniques, specifically convolutional neural networks CNNs, have the capability to routinely acquire and mine complex features from images, making them well-suited for medical imaging tasks, in such redundant problems in accuracy because of feature variations. This optimized method identifying the brain tumors in MRI images dataset collected from standard repository. The proposed approach uses a Stochastic Spin Glass Classifier (SSGC) to automatically learn and classify brain tumor images. The approach includes several essential components based on the features like, texture, shape, projection, region etc. The integration of segmentation, histogram evaluation, feature selection, and classification techniques has shown promising results, outperforming traditional methods and demonstrating potential for enhancing brain tumor detection in MRI images.

2. Related work:

In various review of existing literature indicates that machine learning (ML) and deep learning (DL) approaches hold significant potential for improving the precision and efficiency of brain tumor detection. These approaches could potentially transform the landscape of medical imaging, offering precise and timely diagnoses of brain tumors, ultimately improving patient outcomes. Nevertheless, additional research is required to validate and refine these techniques for clinical application. Several studies have demonstrated the high accuracy of DL models in tumor segmentation and classification.

Prior approaches are based combined feature extraction and classification algorithms to accurately detect and classify brain tumors from MRI images, achieving high sensitivity and specificity in tumor detection. Additionally, another study employed Convolution Neural network (CNN) techniques for brain tumor detection using multi-modal MRI images. The DL model integrated multiple MRI modalities for findings in tumor detection, demonstrating superior performance compared to traditional methods [5].

The typical similitudes of the data of the method proposed for the segmentation of the complete tumor, the nucleus of the tumor, and the tumor with contrast in data of real patients are 0,84, 0,685 and 0,585, respectively [6].This article furnishes peruses with a total outline of the subject and new components of how different AI and picture division approaches are utilized to analyze mind growth.

By contrasting Ensemble Learning (EL) techniques, profound gaining strategies are additionally effective for cancer division from mind X-ray pictures [7].A EL-based technique is introduced to separate necrotic and upgraded growth tissue content, which is significant for the far-reaching assessment of reactions to radiotherapy. Approval concentrates on clinical and manufactured cerebrum cancer informational indexes, uncovering 80% to 90% cross-over execution of the proposed calculation. It underscores its low aversion to seed statements, power to various and heterogeneous growth types, and effectiveness in figuring time [8].The analyses are done utilizing the proposed choice calculation with three classifiers.

The typical arrangement correctness accomplished by the Random Forest approach is 88.43% (KNN), 92.5% (mSVM) and 95.86% (NN), individually. The existing calculations like ICA and GA shows an expansion in exactness of 2% (KNN), 3% (SVM), and 4% (NN). This prior approach beats the NN classifier with 95.86% exactness utilizing heterogeneous elements [9].The attractive reverberation was % and 91.80% on the little X-ray dataset, respectively. The proposed technique is better than existing writing, showing that it very well may be utilized to arrange cerebrum cancers quickly and precisely [10].

The outcomes obtained from the tests show that our model has accomplished better execution than past models. The proposed model is suggested for malignant growth discovery in a clinical Web of Things medical services framework because of its highly predictive outcomes [11]. Specialists often rely upon multimodal mind imaging to break down cerebrum disease, for example, because of information from coronal and sagittal points of view. In existing level multi-view dynamic mix framework to embrace the additional 3D information embedded in such datasets to deal with the introduction of the brain development division [12].

Additionally, the deep recurrent neural network is utilized for tumor classification severity, trained by random forest algorithm [12]. The fractional-CSO demonstrates superior performance in evaluation metrics, achieving 93.35% accuracy, 91% specificity, and 93% sensitivity using the simulated BRATS dataset [14].The improved CNNBCN

model not only delivers successful outcomes in brain tumor image classification but also enhances the neural network design methodology [15]. The datasets consist of 233 and 73 patients, with a total of 3064 and 516 images on T1-weighted contrast-enhanced images for the first and second datasets, respectively. Existing level projects the performance of 92.13% and 91.7% for the two studies. These results highlight the model's capability for multi-classification of brain tumors [16].

The survey outlines potential future directions for research and development in ML-based brain tumor detection, including the integration of multimodal imaging data, transfer learning, and interpretability of ML models. It concludes by emphasizing the transformative potential of ML techniques in advancing brain tumor detection and the need for continued research efforts in this domain[18].

The hostile node detection method is created using classifiers. The characteristics are extracted from the MANET nodes. Each node in a MANET has features that define it. Features separate the trustworthy node from the malevolent network. There are two distinct modes for this classifier: testing and training. The ANFIS classifier, which creates the learned pattern, trains the features that are retrieved from each of the malicious and trustworthy nodes separately during the training phase of the classification. The properties of the specific node that have been retrieved are evaluated in the classifier's testing mode using a learned pattern [26].

Random Forest Classifier (RF)-based evaluation and classification of lesion tissue, a random forest, presumably non-linear layout approach, and a majority controlling numerical classifier are applied. A bottom classifier, R, fuses a DT and creates a large number of decision trees. The results of this prospective model are more precise than those of the manual assessment. Now that clinicians have access to a reliable and skilled computational method for segmenting and classifying lesion sections, they can more accurately estimate how long lesions will heal. Practical accuracy increased by 93.8%. When compared to hand examination, this approach yields the highest accuracy [27].

Table 1. Comparison of different methodologies at the existing level

Author year	Reference	Technique used	Result achieved
S. Mohsen et al.,(2023)	[19]	Hybrid Single Image Super-Resolution	91%
Ç. Özkaya et al.,(2023)	[20]	CNN	89%
S. Solanki et al.,(2023)	[21]	Intelligence Techniques	90%
A. Islam et al.,(2013)	[22]	multifractal feature-based	84%
C. Ma et al.,(2018)	[23]	Random Forests	88%
Rezaei, G et al. (2023)	[24]	PROACT	82%

The study focuses on two aspects. Firstly, the classification of Artificial Neural Network (ANN) and secondly, the introduction of medical technology that can predict clinical diseases comprehensively using ANN technique. ANN method discovers wide applications in the medical field [25]. The review analyzed common image quality assessments like SNR and PSNR to investigate their influence on uniform images [26].

3. Proposed Methodology

Towards the development brain tumor detection using MRI Images using Segmentation, Histogram Evaluation, Feature Selection, and Classification Techniques. First, we pre-process the MRI images to enhance the tumor features and remove noise based on bilateral filter. Then the MRI images are segmented using Active Region Slice window segmentation (ARSW) to identify and isolate the brain tumor regions. The segmented regions are then subjected to histogram evaluation to extract relevant features, such as intensity and texture information. Optimal support scaling vector based feature Selection (OSSCV) Feature selection methods are employed to identify the greatest discriminative features for tumor detection. Finally, stochastic spin-glass model Classification (SSGM) classification model is trained using the selected features to differentiate between tumor and non-tumor regions.

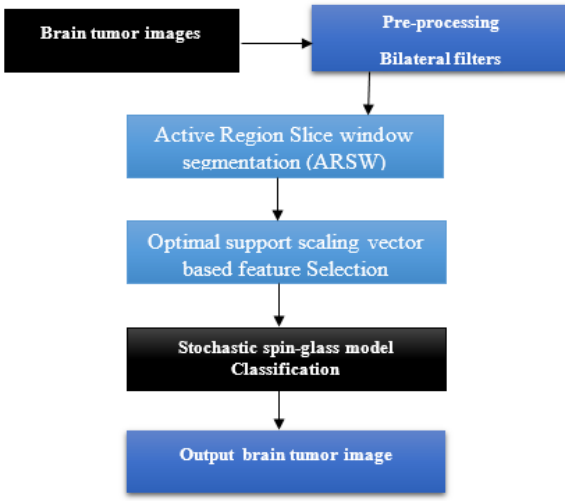

Fig.2 Stochastic spin-glass model classification

The performance of our proposed approach was evaluated by feature selection and classification approach using the MRI images containing dataset including both tumor and non-tumor cases. In this study, we introduce an integrated approach for brain tumor detection in MRI images, combining segmentation, histogram evaluation, feature selection, and classification methods. The integration of these techniques aims to improve the accuracy and efficiency of brain tumor detection, ultimately contributing to better patient care and outcomes. Our experimental results demonstrate that the SSGM model achieves high accuracy in brain tumor detection, outperforming traditional machine learning methods. The proposed approach shows promise in assisting radiologists in diagnosing brain tumors more accurately and efficiently.

3.1 Pre-processing

Initialization is the preprocessing system, it means collecting the disease information from brain tumor dataset. The preprocessing using the Geometric transformations functioning for image width, height, scale, and rotation-based processing of the image and 2D and 3D model-based image splitting and complex transformation are easy to rescale the system and parallel image processing system. The following is the image for the output of the processing of brain tumour 2D and 3D, rescaling the image in Figure 2.

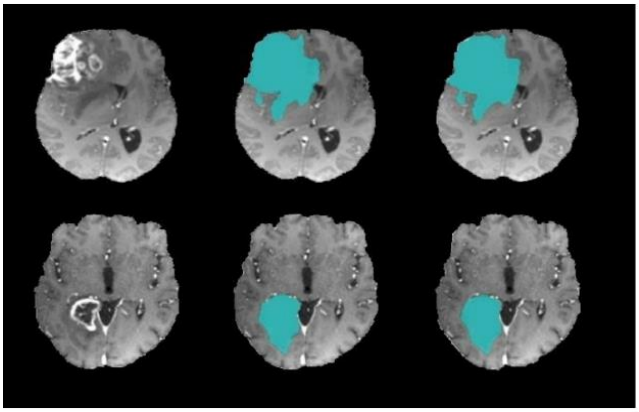

Fig 3. Preprocessing 3D Geometric transformations result

Here, $I(x,y)$is image functions, the order of the geometric moment is given by p+q is point the x and y axis.

$$m_{pq} = \int_{-\infty}^{\infty} \int_{-\infty}^{\infty} x^p, y^p \, I(x,y) dxdy \qquad (1)$$

The geometric moment provides important information for the reconstruction of images. Each coefficient contributes to providing information about the image.

Many classification tasks require variation in the geometric transform. However, a solution can be found by defining invariable moments.

Image Translation

$$x' = x + a \qquad (2)$$
$$y' = y + b \qquad (3)$$

Image Scaling:

$$x' = ax, \quad y' = ay \qquad (4)$$

Image Rotations:

$$x' = cos\theta sin\theta x \qquad (5)$$

$$y' = -sin\theta cos\theta y \qquad (6)$$

The moment of. Geometric transformations are

$$\mu_{pq} = \int \int I(x,y)(x-x)^{-p} (y-y)^{-q} dxdy \qquad (7)$$

Where

$$x = \frac{m_{10}}{m_{00}}, y = \frac{m_{01}}{m_{00}} \qquad (8)$$

$$\eta_{pq} = \frac{\mu_{pq}}{\mu_{00}}, \gamma = \frac{p+q+2}{2} \qquad (9)$$

The following equations represent the image function, digital image I(x, y), i=0, 1…, the corresponding image replacing integrals by summation.

$$m_{pq=\sum_i \sum_j I(x,y) i^p j^q} \qquad (10)$$

Here, equation (10) finally processing is the preprocessing of Geometric transformations.

3.2 Bilateral Filter

A combination of domain and threshold filtering can be referred to as bilateral filtering and returns a pixel value

with the average of neighbouring similar pixel values. Furthermore, pixel values in small neighbourhoods are interdependent to converge the normalized similarity function in smooth areas. Therefore, implementing a standard domain filter based on the bilateral filter and averaging the small, poorly correlated differences between pixel values caused by noise can be recommended. The main feature of this system is to convert the grayscale image of the image using resolution filtering. Furthermore, the filter replaces the central bright pixel with the average of its adjacent bright pixels and ignores the dark pixels.

Estimate the output of the low-pass domain filter applied to the image as shown in Equation 11. Let's assume ξ −near point, c-neighbourhood centre, s- input and output multiband, $x(\xi, c)$-measure the geometric, $N(c)$ −produced filter images, N-range of image function, x-closeness function,

$$s(T) = T_y^{-1}(c) \int_{-\infty}^{\infty} \int_{-\infty}^{\infty} M(\xi)\, x(\xi, c) y_{\xi} (11)$$

Equation 12 shows the computation of the low pass signal components by filtering. Where T_y −constant.

$$T_y(c) = \int_{-\infty}^{\infty} \int_{-\infty}^{\infty} x(\xi, c)\, y_{\xi} \quad (12)$$

Equation 13 is used to evaluate the threshold filtering function of vector difference. Let's assume $T\big(N(\xi), N(c)\big)$ −measure the photometric, T-unbiased function

$$s(c) T_g^{-1}(c) \int_{-\infty}^{\infty} \int_{-\infty}^{\infty} N(\xi)\, T\big(N(\xi), N(c)\big) y_{\xi} \quad (13)$$

Evaluate the normalization constant based on the range of the image function as shown in Equation 4.

$$T_{\mathrm{T}}(c) = \int_{-\infty}^{\infty} \int_{-\infty}^{\infty} T\left(N(\xi), N(N)\right) y_{\xi} \quad (14)$$

Evaluate the geometric and photometric normalization as described in Equation 15 and 16. Let's assume $T(c)$ −normalization weight,

$$s(c) = T^{-1}(x) \int_{-\infty}^{\infty} \int_{-\infty}^{\infty} N(\xi)\, x(\xi, c)\, h\big(N(\xi), N(c)\big) y_{\xi} (15)$$

$$T(c) = \int_{-\infty}^{\infty} \int_{-\infty}^{\infty} x(\xi, c)\, h\big(N(\xi), N(x)\big) d_{\xi} (16)$$

As shown in Equation 17 and 18, estimate the Euclidean distance parameter of the Gaussian function. Where σ_y −geometric spread,

$$x(\xi, c) = m^{\frac{1}{2}\left(\frac{y(\in, c)}{\sigma_y}\right)^2} (17)$$

$$y(\xi, c) = y(\xi - c) = \|\xi - c\| (18)$$

Compute the similarity function between Euclidean distances as shown in Equation 19 and 20. Let's assume $h(\xi, c)$ −gaussian function, c and ξ -Euclidean distance.

$$h(\xi, c) = m^{\frac{1}{2}\left(\frac{\delta(N(\xi).N(c))}{\sigma^{\mathrm{T}}}\right)^2} (19)$$

$$\delta(\varphi, f) = \|\varphi - f\| (20)$$

In Equation 21 and 22, calculate the threshold filtering of the simple transform of the gray levels. Let's assume φ, N −intensity value, $\nu(\varphi)$ −frequency distribution grey level, φ −grey value, $\mathrm{T}(\varphi, N)$-mapping kernel, $\nu(N)$ −histogram, N-normalized unit area, T −density function,

$$s = \int_0^{\infty} \varphi\, \mathrm{T}(\varphi, N) y_{\varphi} (21)$$

$$\mathrm{T}(\varphi, N) = \frac{h(\varphi, N)\nu(\varphi)}{\int_0^{\infty} s(\varphi, N)\nu(\varphi)} y_{\varphi} (22)$$

In this category, bilateral filtering proved to be useful in terms of analyzing the characteristics of the grayscale transformation.

3.3 Active Region Slice window segmentation

The planted surfaces finally begin to expand and solidify. The proposed approach performs similarly to its well-known cousin, according to experimental findings. Images hardly ever feature RGB colors, and this is crucial for converting color spaces into other spaces. The most crucial application of picture segmentation is for image color spaces, where it can produce superior outcomes.

There are two ways of seed selection: non-edge and smoothing. First, our discussion about the non-edge detection algorithm the canny is the best edge detection for image processing, and a gradient histogram is used to achieve the threshold of the competent operators. The best choice for the greyscale image is better for edge detection and image segmentation because the gray scale can give the best results. To perform the good segmentation. There are select the two gray scale images one C0 and C1.here two values are calculated by

$$\mu_0(T) = \frac{1}{w_0} \sum_{o<k<255} k.p(k) \quad (23)$$

$$\mu_1(T) = \frac{1}{w_1} \sum_{o<k<255} k.p(k) \quad (24)$$

Here μ_0, μ_1 is mean by$C_0 and C_1$, there are mean values calculated by them

$$\mu(T) = w_0\mu_0(T) + w_1\mu_1(T) \quad (25)$$

Here define the w_0 and w_1 are probability of $C_0 and C_1$ and μ is the image, our calculated by the variance

$$G(T) = w_0(\mu - \mu_0)^2 + w_1(\mu - \mu_1)^2 \quad (26)$$

Apply for Otsu methods, calculate the best threshold values as follows.

$$g = arg_{0<T<255}^{max}[G[T]] \quad (27)$$

Here G is the corresponding values of largest, T is the minimum probability of misclassification, the Otsu is calculate the smallest values of misclassification, Otsu have given the more accurate of threshold, but canny

operator can use of high the sold, and low threshold 0.4 values is high.

$$\begin{cases} h = T \\ l = 0.4T \end{cases} \quad (28)$$

Here h and l is the high threshold values, the algorithm steps as follows

Step1 image color changed into gray scales

Step2 apply the Otsu method to maximum value of cluster variance threshold T.

Step3 equation (28) achieved low and high threshold edges $X^x y$ and gray scale image values is 0.1 is edge point.

3.4 Histogram color quantization

The color variation handled to separate the pixel points in the tumor regions are covered. The candidate must select higher values than the neighbors; the Manhattan distances of the RGB have been calculated as

$$\|x - x_c\| = \sum_{i=1}^{3} |x_i - x_c| \quad (29)$$

Here the values of RGB and xc is middle point, the extended distance is

$$\mu = \underset{i=1\ldots8}{Max} \|x - x_c\| \quad (30)$$

$$\mu < T1 \quad (31)$$

Here T1 have a predefined threshold values and $X^x y$ is smoothing values, 26 quantization levels of RGB total color is 17576, maximum RGB color resolution is 17000 only.

Let l, k is the neighboring region, the two adjacent region distance is calculate as follows:

$$d = \sqrt{((R_l^e - R_k^e)^2 + (G_l^e - G_l^e)^2 + (B_l^e - B_k^e)^2} \quad (32)$$

Here $d = \sqrt{((R_l^e - R_k^e)^2 + (G_l^e - G_l^e)^2 + (B_l^e - B_k^e)^2}$ is main values of the region and l and k is respectively

3.5 Optimal support scaling vector based feature Selection (OSSCV)

The feature selection is an extract of the image from the image dataset. Function for image filtering and matching image selection, correct diseases affected images and no diseases affected images are filtered after that classification. Feature selection using a powerful machine learning method is used here. Here, W is the collection of input datasets.

Let $d(x_i, y_i)| < | < W$ is training of w each images samples $x_i \in L^d$ each label class$y_i \in \{1, -1\}$, m_{pq} is Geometric transformations of the images.

Here d the feature selection images. This volume to finding w and b so that

$$y_i(w.x_i + m_{pq}) > 0, i = L \ldots W \quad (33)$$

Rescaling the images of w and b so that

$$max_{;<j<W}^{y_i(w.x_i+c)>0, i=l\ldots W} \quad (34)$$

So the close-set image comparison equation (34) hyper planes of distance

$$y_{\,i}(w.x_i + m_{pq}) > L \quad (35)$$

Here, find the optimal separating hyper plane (OSH) and closed set of distance w

$$\frac{1}{||W||} = \frac{1}{4}||W||^2 \quad (36)$$

Maximizing the amount of is under constraints $||W||^2$ is under linear constraints equations (36) achieved with the multipliers. Denote by $\alpha = (\alpha_1 \ldots \alpha_N)$ the W non-negative multiplier associated, optimization problem solved to normalization of the image

$$W(\alpha) = \sum_{i=0}^{W} \alpha_i - \frac{1}{2}\sum_{i=0}^{N} \alpha_i, \alpha_j, y_i, y_j x_i . x_j + m_{pq} \quad (37)$$

Here $\sum_{i=0}^{N} y_i \alpha_i$ is achieved by the normal programming Method. We denote the $\alpha^0 = (\alpha^0{}_1 \ldots \alpha^0{}_N)$is solution for maximum problem (37) found. Here (w^0, b^0) the following expression is

$$w_0 = \sum_{i=0}^{W} \alpha^0 y_i x_i + m_{pq} \quad (38)$$

Feature weights for which $\alpha_i > 0$ is satisfy the equation (38) with equality.From equation (39), the overexcited decision plane is to be written as

$$f(x) = sign[\sum_{i=0}^{W} \alpha^0 y_i x_i + w_0] + m_{pq} (39)$$

The input images are calculated, and the high-dimensional feature has been selected here

Change x is feature selection $\emptyset(x), taken$ equation (40) combined here.

$$W(\alpha) = \sum_{i=0}^{W} \alpha_i - \frac{1}{2}\sum_{i=0}^{N} \alpha_i, \alpha_j, y_i, y_j \emptyset x_i . \emptyset x_j + m_{pq} \quad (40)$$

Here, equations (36) and (37) select the feature selection images $W(\alpha)$ selects the image feature selection of the images

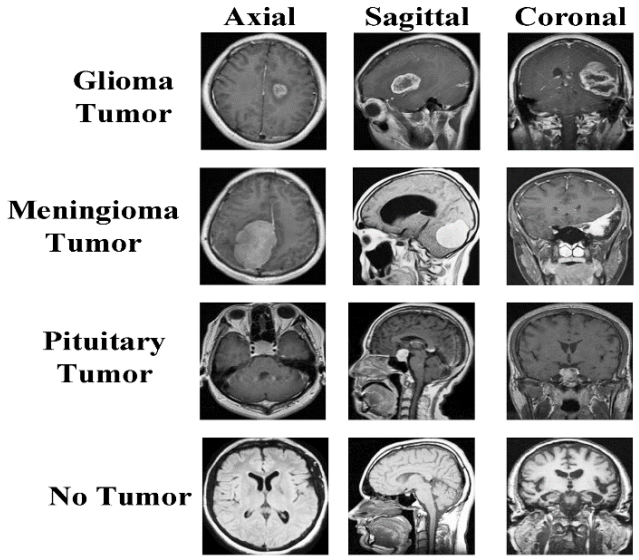

Fig 4. Feature selection

Discuss about the figure.4 display the feature selection or extraction image form dataset. The feature selection select the essential features like shape, size of the tumor, length etc. The images displayed into various types of brain tumor diseases.

Stochastic spin-glass model is a counterfeit brain network utilized for neural learning. The projection of feature difference presence in the image can be extracted from the images, such as intensity, texture, and shape features. These features can be considered as analogous to the "spins" in a spin-glass system, with each feature representing a different aspect of the image. The stochastic nature of spin-glass systems involves random fluctuations and dynamics of region classification. In the stochastic aspect use of randomization and probabilistic methods in the feature extraction label to the classification process. This could involve incorporating stochastic gradient descent, dropout layers within a neural network architecture.

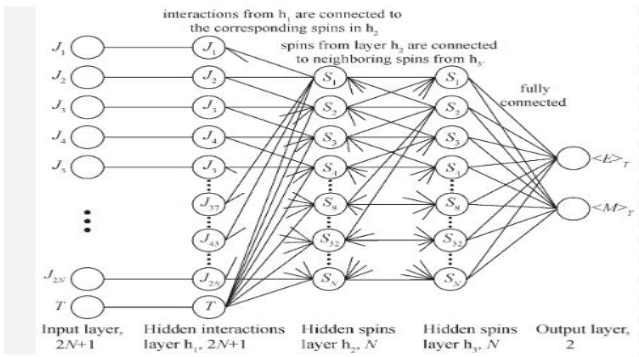

Fig 5. Stochastic spin-glass model flow structure

Here figure.5 define the flow structure proposed system, and v1,v2,v3 is visible unit of the image layer and w1,w2,,w3,w4 is hidden unit of the image processing layers. Stochastic spin-glass model Create s feature dependencies based extraction forming from tumor texture regions input to the classification of the brain tumor disease prediction under the validation of testing training images. The input classification images are W1, W2...Wn. The rough energy landscape of a spin-glass system could be analogized to the complex and high-dimensional feature space in image processing. The classification task involves navigating this feature space to discriminate between tumor and non-tumor regions, akin to finding the low-energy states in a spin-glass system.

$$W = W(\alpha) + [\mathrm{W}(1,\mathrm{w}) = \ \mathrm{W1}\ldots.+\mathrm{C}]\epsilon spin^{k*d}(41)$$

The intersection filter is applied to each window, resulting in scalar values ri, each for the ith window:

$$r_i = g(x_i, u)\epsilon spin + W(\alpha) \quad (42)$$

In repetition one normally relates extra filters, u1….. un, which can then be denoted as a vector increased by a matrix U and with an addition of term b:

$r_i = g(x_i.U + C)$+$W(\alpha)$(43)Discuss about the figure 5 is Stochastic spin-glass model for classification of the brain tumor image, and first feature selection of the images and then classification the tumor images. Finally detection for tumor images in class by labels With

$$r_i \in R^l, x_i \in R^{(k*d)}, U \in spin^{(k,d*l)} and b \in spin^L$$
(44)

After applying filter on images, it returns m vector w, after applying it on post tags, it returns m equal vectors for shape and again m vectors.

$$P_i = images_{l:m} + Tranformation_{l:m} \quad (45)$$

Or by concatenation

$$P_i = [image_{l:m} + width_{l:m} + size_{l:m}]\ )(46)$$

Equations (45) and (46) the classification process could be viewed as exhibiting glassy behavior, where the system explores different configurations of features to arrive at a decision. The presence of noise, uncertainty, and the need for robust decision-making in the presence of complex and overlapping features can be likened to the glassy behavior of a spin-glass system. The exploration of different feature configurations and the optimization of the classification model could be framed within the context of exploring the energy landscape of a spin-glass system. This could involve leveraging optimization algorithms inspired by spin-glass theory or exploring the use of unconventional optimization techniques that mimic the stochastic exploration of spin configurations finally classify the brain tumor classification to produce the best accuracy prediction result.

4. Result and Discussion

The results of our study highlight the potential of DL-based approaches in improving brain tumor detection in MRI images. The use of SSGM for automatic feature learning and classification has shown promising results, indicating the potential for enhancing the diagnostic process for brain tumors. The proposed approach has the potential to assist radiologists in making more accurate and timely diagnoses, ultimately leading to improved patient outcomes.

The proposed system of spin classification algorithm compared to CNN, Ensemble method, Random forest. The proposed system of SSGM accuracy and Precision, recall, and F1-measure for the best result of the classification and result found using the language of Python and the tool of anaconda for developed the classification result. Figure 6 discusses the Training validation loss accuracy and the accuracy loss compared to various limitations 40 number of all epochs in training. These 2 epochs are loss accuracy. The first round of loss accuracy is 42.86%, and the second round is 56.69%. Figure 7 discusses the testing validation loss accuracy, the accuracy loss compared to various limitations 40 number of all epochs in training. Figure 8 discuss about the confusion matric of brain tumor diseases feature.

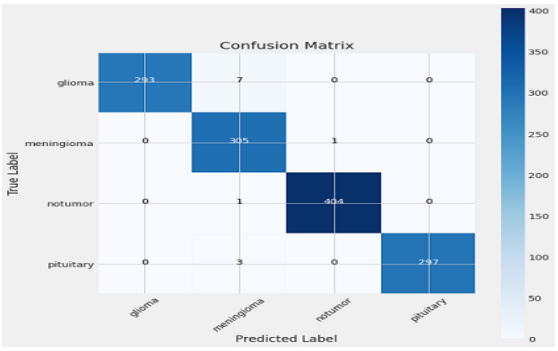

Fig 6. Confusion matrix for brain tumor diseases

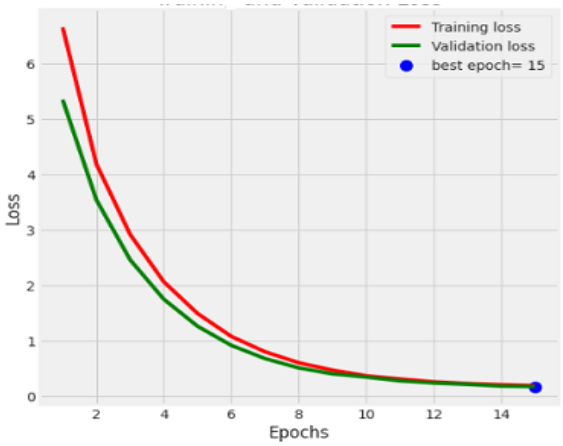

Fig 7. Training validation loss accuracy

Fig 8. Testing validation accuracy

Figure.8 discuss the testing validation accuracy and the accuracy loss compared to various limitation of 40 number of all epochs in testing. These 2 epochs are testing accuracy. The first round of testing accuracy is 0.86, and the second round is 0.90. Figure. 8 discuss the testing validation loss accuracy and the accuracy loss compared to various limitation of 40 number of all epochs in testing. These 2 epochs' test accuracy in the first round of Validation testing was 0.1663, and in the second round of testing, Validation Accuracy was 0.9908.

Table.2 Experiment Result for SSGM Performance Error Rate

Methods	Error Rate (%)
CNN	64.2
ENSEMBLE	52.9
RANDOM FOREST	40.89
PROPOSED	26.48

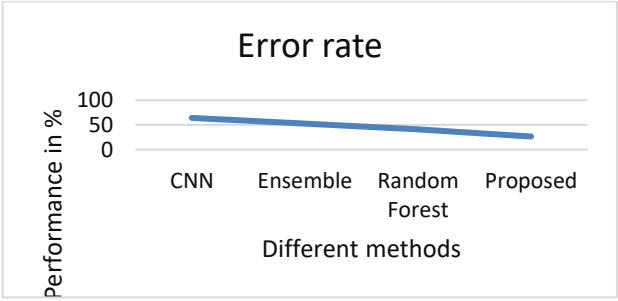

Fig 9. SSGM Methods of Error rate

Discussion about table.1 and Figure 9 is method accuracy; the performance of the CNN method Error rate is 64.2%, the performance of the Ensemble method Error rate is 52.9%, the performance of the random forest method Error

rate is40.89%, and the proposed system of SSGM Error rate is 26.48%.

$$precision = \frac{True\ positive}{ture\ positive + False\ positive} \quad (47)$$

Discussion about Figure.9 and table.3 is method accuracy, the performance of the CNN method Performance precision is 92.5%, the performance of the Ensemble method Performance precision and 93.5%, and the performance of the Random Forest method Performance precision is 94.5%. The proposed SSGM Performance precision and is 96.5%, and the best result could classify the SSGM methods.

The proposed system $precision = 96.5\%$

Table 3. Precision Accuracy

Methods	Precision Accuracy (%)
CNN	92.5
Ensemble	93.5
Random Forest	94.5
SSGM	96.5

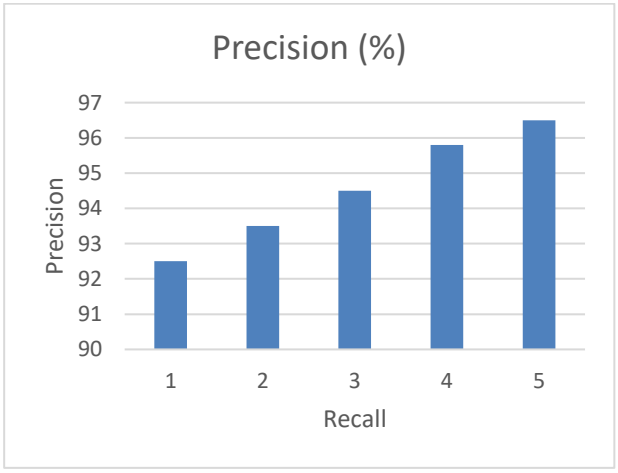

Fig 10. Experiment Result for SSGM Performance precision and recall

Discussion about Figure.10 and table.4 is Recall accuracy, the performance of the CNN method Performance Recall is 91.5%, the performance of the Ensemble method Performance Recall is 92.5%, and the performance of the Random Forest method Performance Recall is 93.5%. The proposed SSGM Performance precision and is 95.5%, and the best result could classify the SSGM methods.

$$Recall = \frac{TruePositive}{Truepositive + FalseNagative} \quad (48)$$

The proposed system of Recall =95.5%

Table 4. Recall Precision

Methods	Recall (%)
CNN	91.5
Ensemble	92.5
Random Forest	93.5
SSGM	95.5

Discussion about Figure.11 and table.5 is method Performance F1- Measure, the performance of CNN method Performance F1- Measure is 91.4% and performance of Ensemble method Performance F1-Measure is 92.5%, and the performance of Random Forest method PerformanceF1- Measure is 93.7%, and the proposed system of SSGM Performance F1- Measure is 96.1%. The best result could be to classify the SSGM methods.

$$F1\ Score = 2.\frac{Precision * Recall}{Precision + Recall}$$

$$F1\ Score = 96.1\%$$

Table 5. $F1\ Score$

Methods	$F1\ Score$ (%)
CNN	91.4
Ensemble	93.5
Random Forest	93.7
SSGM	96.1

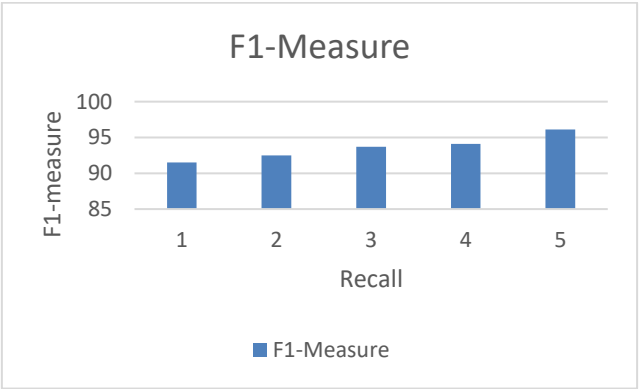

Fig 11. Experiment Result for SSGM Performance F1-Measure

5. Conclusion

In conclusion, the proposed Stochastic Spin-Glass Model Classification (SSGM) approach for brain tumor detection using MRI images. The experimental results demonstrate the efficacy of the proposed method in achieving high

accuracy in brain tumor detection. The use of CNNs for automatic feature learning and classification has the potential to assist radiologists in diagnosing brain tumors more accurately and efficiently, ultimately leading to improved patient outcomes. Further research and validation on larger and diverse datasets to produce best accuracy in testing and validation accuracy. The proposed SSGM Performance precision is 95.5%, with the best outcome being a classification of the SSGM techniques. Performance F1- Measure, CNN technique performance F1- Measure is 91.4%, and Ensemble technique performance F1- Measure is 92.5%, and Random Forest technique performance 93.7% is the performance F1-Measure, and the SSGM system is suggested 96.1% is the performance F1-measure. The classification of SSGM techniques might yield the greatest results

References

[1] S. Bauer, C. May, D. Dionysiou, G. Stamatakos, P. Buchler and M. Reyes, "Multiscale Modeling for Image Analysis of Brain Tumor Studies," in IEEE Transactions on Biomedical Engineering, vol. 59, no. 1, pp. 25-29, Jan. 2012, doi: 10.1109/TBME.2011.2163406.

[2] A. Islam, S. M. S. Reza and K. M. Iftekharuddin, "Multifractal Texture Estimation for Detection and Segmentation of Brain Tumors," in IEEE Transactions on Biomedical Engineering, vol. 60, no. 11, pp. 3204-3215, Nov. 2013, doi: 10.1109/TBME.2013.2271383. .

[3] A Song, P. Wen, T. Ahfock and Y. Li, "Numeric Investigation of Brain Tumor Influence on the Current Distributions During Transcranial Direct Current Stimulation," in IEEE Transactions on Biomedical Engineering, vol. 63, no. 1, pp. 176-187, Jan. 2016, doi: 10.1109/TBME.2015.2468672.

[4] A.Ma, G. Luo and K. Wang, "Concatenated and Connected Random Forests With Multiscale Patch Driven Active Contour Model for Automated Brain Tumor Segmentation of MR Images," in IEEE Transactions on Medical Imaging, vol. 37, no. 8, pp. 1943-1954, Aug. 2018, doi: 10.1109/TMI.2018.2805821.

[5] A.I. Zacharaki, D. Shen, S. -K. Lee and C. Davatzikos, "ORBIT: A Multiresolution Framework for Deformable Registration of Brain Tumor Images," in IEEE Transactions on Medical Imaging, vol. 27, no. 8, pp. 1003-1017, Aug. 2008, doi: 10.1109/TMI.2008.916954.

[6] M. Huang, W. Yang, Y. Wu, J. Jiang, W. Chen and Q. Feng, "Brain Tumor Segmentation Based on Local Independent Projection-Based Classification," in IEEE Transactions on Biomedical Engineering, vol. 61, no. 10, pp. 2633-2645, Oct. 2014, doi: 10.1109/TBME.2014.2325410.

[7] T. A. Soomro et al., "Image Segmentation for MR Brain Tumor Detection Using Machine Learning: A Review," in IEEE Reviews in Biomedical Engineering, vol. 16, pp. 70-90, 2023, doi: 10.1109/RBME.2022.3185292.

[8] AHamamci, N. Kucuk, K. Karaman, K. Engin and G. Unal, "Tumor-Cut: Segmentation of Brain Tumors on Contrast-Enhanced MR Images for Radiosurgery Applications," in IEEE Transactions on Medical Imaging, vol. 31, no. 3, pp. 790-804, March 2012, doi: 10.1109/TMI.2011.2181857.

[9] Vidyarthi, R. Agarwal, D. Gupta, R. Sharma, D. Draheim and P. Tiwari, "Machine Learning Assisted Methodology for Multiclass Classification of Malignant Brain Tumors," in IEEE Access, vol. 10, pp. 50624-50640, 2022, doi: 10.1109/ACCESS.2022.3172303.

[10] S. Asif, W. Yi, Q. U. Ain, J. Hou, T. Yi and J. Si, "Improving Effectiveness of Different Deep Transfer Learning-Based Models for Detecting Brain Tumors From MR Images," in IEEE Access, vol. 10, pp. 34716-34730, 2022, doi: 10.1109/ACCESS.2022.3153306.

[11] A.U. Haq et al., "IIMFCBM: Intelligent Integrated Model for Feature Extraction and Classification of Brain Tumors Using MRI Clinical Imaging Data in IoT-Healthcare," in IEEE Journal of Biomedical and Health Informatics, vol. 26, no. 10, pp. 5004-5012, Oct. 2022, doi: 10.1109/JBHI.2022.3171663.

[12] Y. Ding et al., "MVFusFra: A Multi-View Dynamic Fusion Framework for Multimodal Brain Tumor Segmentation," in IEEE Journal of Biomedical and Health Informatics, vol. 26, no. 4, pp. 1570-1581, April 2022, doi: 10.1109/JBHI.2021.3122328.

[13] S. Huda, J. Yearwood, H. F. Jelinek, M. M. Hassan, G. Fortino and M. Buckland, "A Hybrid Feature Selection With Ensemble Classification for Imbalanced Healthcare Data: A Case Study for Brain Tumor Diagnosis," in IEEE Access, vol. 4, pp. 9145-9154, 2016, doi: 10.1109/ACCESS.2016.2647238.

[14] Z. Huang et al., "Convolutional Neural Network Based on Complex Networks for Brain Tumor Image Classification With a Modified Activation Function," in IEEE Access, vol. 8, pp. 89281-89290, 2020, doi: 10.1109/ACCESS.2020.2993618.

[15] A.Kujur, Z. Raza, A. A. Khan and C. Wechtaisong, "Data Complexity Based Evaluation of the Model

Dependence of Brain MRI Images for Classification of Brain Tumor and Alzheimer's Disease," in IEEE Access, vol. 10, pp. 112117-112133, 2022, doi: 10.1109/ACCESS.2022.3216393.

[16] R. Cristin, K. S. Kumar and P. Anbhazhagan, "Severity Level Classification of Brain Tumor based on MRI Images using Fractional-Chicken Swarm Optimization Algorithm," in The Computer Journal, vol. 64, no. 10, pp. 1514-1530, June 2021, doi: 10.1093/comjnl/bxab057.

[17] H. H. Sultan, N. M. Salem and W. Al-Atabany, "Multi-Classification of Brain Tumor Images Using Deep Neural Network," in IEEE Access, vol. 7, pp. 69215-69225, 2019, doi: 10.1109/ACCESS.2019.2919122.

[18] J. J. Corso, E. Sharon, S. Dube, S. El-Saden, U. Sinha and A. Yuille, "Efficient Multilevel Brain Tumor Segmentation With Integrated Bayesian Model Classification," in IEEE Transactions on Medical Imaging, vol. 27, no. 5, pp. 629-640, May 2008, doi: 10.1109/TMI.2007.912817.

[19] S. Mohsen, A. M. Ali, E. -S. M. El-Rabaie, A. ElKaseer, S. G. Scholz and A. M. A. Hassan, "Brain Tumor Classification Using Hybrid Single Image Super-Resolution Technique With ResNext101_32× 8d and VGG19 Pre-Trained Models," in IEEE Access, vol. 11, pp. 55582-55595, 2023, doi: 10.1109/ACCESS.2023.3281529.

[20] Ç. Özkaya and Ş. Sağiroğlu, "Glioma Grade Classification Using CNNs and Segmentation With an Adaptive Approach Using Histogram Features in Brain MRIs," in IEEE Access, vol. 11, pp. 52275-52287, 2023, doi: 10.1109/ACCESS.2023.3273532.

[21] S. Solanki, U. P. Singh, S. S. Chouhan and S. Jain, "Brain Tumor Detection and Classification Using Intelligence Techniques: An Overview," in IEEE Access, vol. 11, pp. 12870-12886, 2023, doi: 10.1109/ACCESS.2023.3242666.

[22] A. Islam, S. M. S. Reza and K. M. Iftekharuddin, "Multifractal Texture Estimation for Detection and Segmentation of Brain Tumors," in IEEE Transactions on Biomedical Engineering, vol. 60, no. 11, pp. 3204-3215, Nov. 2013, doi: 10.1109/TBME.2013.2271383.

[23] A.Ma, G. Luo and K. Wang, "Concatenated and Connected Random Forests With Multiscale Patch Driven Active Contour Model for Automated Brain Tumor Segmentation of MR Images," in IEEE Transactions on Medical Imaging, vol. 37, no. 8, pp. 1943-1954, Aug. 2018, doi: 10.1109/TMI.2018.2805821.

[24] G. Rezaei, H. Gholami, M. R. Tootoonchi, and Dehbozorgi, M. H. (2023). Improving the Performance of Gas Extraction by Reducing the Shutdown Time Using an RCA-based Approach–A Case Study. *Journal of Advanced Research in Technology and Innovation Management*, *4*(1), 1–14.

[25] R. Parveen, M. Nabi, F. A. Memon, S. Zaman and M. Ali, "A Review and Survey of Artificial Neural Network in Medical Science", Journal of Advanced Research in Computing and Applications, Vol. 3, No. 1. pp. 7-16, 2016.

[26] Gopalakrishnan Subburayalu, Hemanand Duraivelu, Arun Prasath Raveendran, Rajesh Arunachalam, Deepika Kongara & Chitra Thangavel. "Cluster based malicious node detection system for mobile Ad-Hoc network using ANFIS classifier", Journal of Applied Security Research, 2021.

[27] Chitraa. T, Sundara. C, Gopalakrishnan. S, "Investigation and classification of chronic wound tissue images using random forest algorithm (RF)", no. 1, pp. 643–651, 2022.